






# Photon-gated foldaxane assembly/disassembly†

 Cite this: *Chem. Commun.*, 2024, 60, 8415

 Chenhao Yao,‡<sup>a</sup> Bappaditya Gole, <sup>‡§</sup> Anh Thy Bui, <sup>b</sup> Brice Kauffmann, <sup>c</sup> Ivan Huc, <sup>d</sup> Nathan D. McClenaghan <sup>\*b</sup> and Yann Ferrand <sup>\*a</sup>

 Received 29th June 2024,  
 Accepted 15th July 2024

DOI: 10.1039/d4cc03218g

rsc.li/chemcomm

**Integrating multiple anthracene motifs into aromatic oligoamide sequences gives rise to photoactive foldamers that can sequester a molecular thread forming helix-on-axle assemblies. Photoirradiation is shown to distort the helical host and drive dissociation of the supramolecular assembly and thread liberation as signalled by a photonic output, while thermal reversion regenerates the assembly.**

Aromatic oligoamide foldamers have emerged as a versatile class of functional molecules, which adopt robust folded conformations whose properties can be finely tuned based on the chosen sequence of monomers.<sup>1</sup> Judicious design of such foldamers has been shown to offer cavities for strong and selective binding of a range of guest molecules<sup>2</sup> and, more recently, photoactivity has been introduced both in terms of emission and photoreaction.<sup>3</sup> Foldaxanes,<sup>4,5</sup> supramolecular architectures comprising aromatic helices on a linear molecular axle, represent a recent addition to the field of interpenetrating molecules.<sup>6</sup> Reported examples focus on their formation evoking specific complementary hydrogen-bonding motifs and on-axle helix translation dynamics<sup>7</sup> and assembly rates.<sup>7,8</sup> Herein, we consider a supramolecular two-component system, where light can be used to both control the assembly and act as a signalling mechanism of association (or dissociation)

through a fluorescence output. This functioning is reminiscent of a 2-stroke molecular piston,<sup>9</sup> based on a unique foldaxane architecture, combining both light- and thermally-driven steps.

In the current design, as shown schematically in Fig. 1, an unbound T-shaped guest is anticipated to give a specific optical response, a characteristic exciplex emission resulting from an intramolecular interaction between an amine (green) and a fluorophore (blue). Binding and interpenetration within a helix-sheet-helix foldamer<sup>3,10</sup> would result in the guest adopting a more extended conformation, spatially decoupling amine and fluorophore and modulating the observed emission. While a light output would signal the state of the system, a light input could also drive guest photoexpulsion based on steric demands mediated by a reversible  $[4\pi+4\pi]$  photocycloaddition reaction. The structural formulas of molecules developed and studied herein (Fig. 2), include a symmetrical host sequence **1**, integrating diazaanthracene units in a bent three stranded sheet  $A^F-T-A^H-T-A^F$ , flanked with two helical segments comprising a tetrameric amide sequence of 7-amino-8-fluoro-2-quinolinecarboxylic acid ( $Q^F_4$ ) providing a cylindrical cavity which is large enough to accommodate a linear alkyl chain. Terminal polar pinchers ( $P_3$ ) comprising

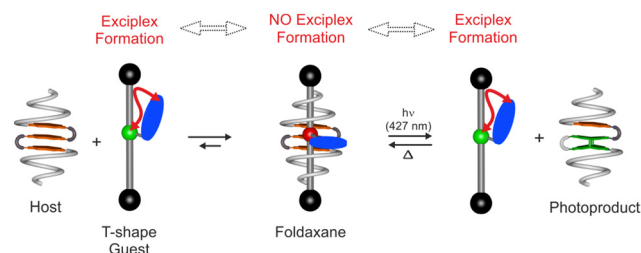


**Fig. 1** Schematic representation of the equilibrium of the self-assembly of helix-sheet-helix host and T-shape guest to form the foldaxane (left) and reactions involved in the photoswitchable process (right). The photo-reaction and thermal reversion can control the release and uptake of the guest, respectively. The free T-shape rod can form an intramolecular exciplex, interacting groups denoted by a red arrow, which will be disrupted in the foldaxane.

<sup>a</sup> Univ. Bordeaux, CNRS, Bordeaux INP, CBMN (UMR 5248), 2 rue Escarpit, 33600 Pessac, France. E-mail: yann.ferrand@u-bordeaux.fr

<sup>b</sup> Univ. Bordeaux, CNRS, Institut des Sciences Moléculaires (UMR5255), 351 cours de la Libération, 33405 Talence cedex, France. E-mail: nathan.mcclenaghan@u-bordeaux.fr

<sup>c</sup> Univ. Bordeaux, CNRS, INSERM, Institut Européen de Chimie Biologie (UAR3033/US001), 2 rue Escarpit, 33600 Pessac, France

<sup>d</sup> Department of Pharmacy Ludwig-Maximilians-Universität München Butenandtstr. 5–13, 81377 Munich, Germany

† Electronic supplementary information (ESI) available. CCDC 2162063. For ESI and crystallographic data in CIF or other electronic format see DOI: <https://doi.org/10.1039/d4cc03218g>

‡ C. Y. and B. G. contributed equally.

§ Current address: Department of Chemistry, School of Natural Sciences, Shiv Nadar Institution of Eminence, Greater Noida, Uttar Pradesh 201314, India.



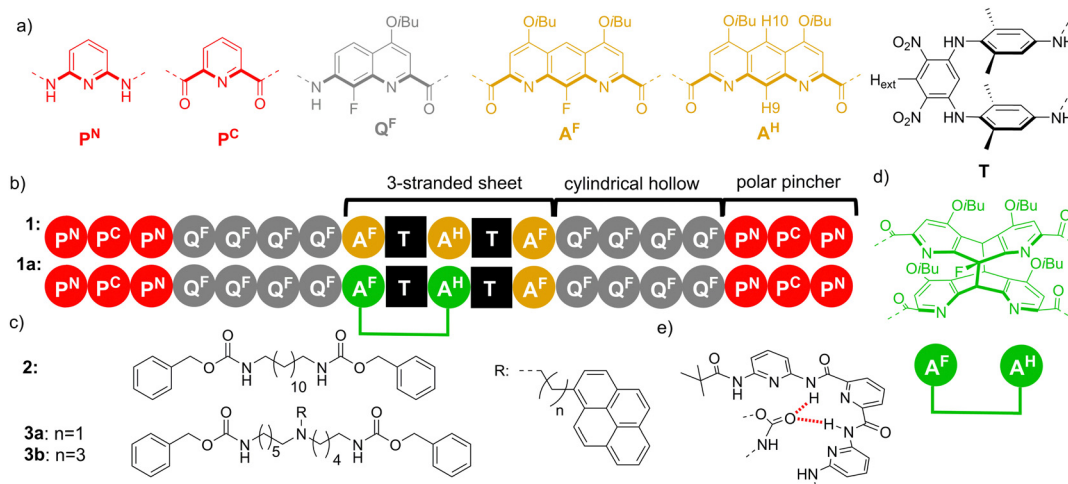


Fig. 2 Representation of: (a) colour formula and letter of the diamine, diacid and amino acid monomers. (b) Oligoamide sequences of **1** and **1a**. Note that **1a** is the photoproduct arising from **1**. (c) Formula of linear guest **2** and T shape guest **3**. (d) A parallel diazaanthracene photoproduct in the aromatic sheet. (e) Binding mode of a carbamate in a polar pincher. The binding is stabilised by intermolecular hydrogen bonds (dotted red lines).

pyridine dicarboxamides are capable of binding to each carbonyl of the guest. Sequence **1a** corresponds to a photoproduct implying a photocycloisomerisation of two parallel anthracene-like moieties, while **2** is a symmetrical dye-free thread.

Helix-sheet-helix **1** was obtained *via* a convergent synthetic strategy, as detailed in the ESI<sup>†</sup> (Schemes S1–S3). Briefly, the conical P<sub>3</sub>Q<sub>4</sub><sup>F</sup> segment was first prepared and transiently functionalised with a labile dimethoxybenzyl (DMB) group able to prevent the aggregation of the aromatic strands during the synthesis.<sup>11</sup> The amino group of the helical segment was connected at each end of the A<sup>F</sup>–T–A<sup>H</sup>–T–A<sup>F</sup> bent sheet diacid and after purification the two DMB groups were removed under acidic conditions.

Evidence for host–guest association in solution was provided by <sup>1</sup>H NMR spectroscopy in CD<sub>2</sub>Cl<sub>2</sub> (Fig. 3a–d). Mixing **1** with a linear **2** or T-shaped **3a** thread led to significant deshielding of N–H proton resonances, indicative of hydrogen bonding between the carbamate groups of the thread and the amide groups of the host located in the terminal P<sub>3</sub> polar pinchers, as represented in Fig. 2e. The NMR spectrum of complex **1**⊃**3** was globally similar to that of aforementioned **1**⊃**2**, but given the non-symmetrical nature of the thread and hence non-equivalence of these functional groups, the number of resonances was doubled. Equally, shifting of aromatic proton signals associated with the foldamer was observed upon binding. In particular, shifts of CH aromatic protons from both the T turn unit (H<sub>ext</sub>) and protons on the central ring of the A<sup>H</sup> unit (H9 and H10) were diagnostic of strong interaction and modification of the internal cavity environment.

Titration of host **1** with guest **2** in CD<sub>2</sub>Cl<sub>2</sub> gave an affinity constant ( $K_a$ ) of  $6.47 \times 10^4$  L mol<sup>-1</sup> and a 1:1 stoichiometry, while a slightly lower value of  $2.63 \times 10^4$  L mol<sup>-1</sup> was obtained for **1**⊃**3a** (Fig. S1–S3, ESI<sup>†</sup>). A single crystal X-ray analysis of **1**⊃**3a** (Fig. 3e–g and Fig. S4, ESI<sup>†</sup>) gave conclusive evidence of the interpenetrating nature of the foldamer assembly and indications on the key binding features. Short C=O...H–N

contact distances of 2.13 Å and 2.06 Å designate the carbamate interaction with the polar pinchers, while the pendant pyrene sub-unit occupied the void in the helical backbone. Additionally, in **1**⊃**3a** the  $\pi$ -system of the appended pyrene adopted a face-to-face orientation with a proximal electron-poor dinitroaromatic of one of the turn units T, which is consistent with the shielding of the H<sub>ext</sub> proton resonance (Fig. 3c vs. Fig. 3b, triangles).

Concerning the optical properties of **3a** and **3b**, the parent 1-alkylpyrene chromophore typically gives intense structured absorption and fluorescence in the near UV spectral region.<sup>12</sup> However, incorporating such a fluorophore into the thread *via* an alkyl tether in close proximity to a tertiary amine group may be anticipated to modify the observed excited-state properties. Indeed, thermodynamically and kinetically-favourable photo-induced electron transfer may occur from amines to excited fused aromatics across simple methylene spacers, as popularised by de Silva and coworkers,<sup>13</sup> whereas when longer linkers are incorporated different responses may be observed. Notably, De Schryver and coworkers showed that an *N*-pyrene excited-state complex/excimer was observed in specific cases in solvents of low-to-medium polarity, and optimal with 2 or 3 methylene group spacers.<sup>14</sup> Disruption of the excimer on foldamer formation, as well as modulation of electronic energy transfer, was targeted as the optical signalling mechanism in the current work and as such, **3a** and **3b** integrating a 2 and 4-methylene spacer, respectively, between amine and pyrene were synthesised. In homogeneous and dilute chloroform (or dichloromethane) solution, structured fluorescence as well as a dominant broad lower energy emission band was observed in the case of **3a** in toluene and dichloromethane solvents ( $\phi_F = 0.26$ ) but is greatly diminished in intensity in highly polar DMSO (Fig. S5, ESI<sup>†</sup>). Further, varying concentration had minimal effect on the relative intensities of each emission band in **3a** consistent with the emission being intramolecular in origin, ruling out excimer formation at these concentrations.



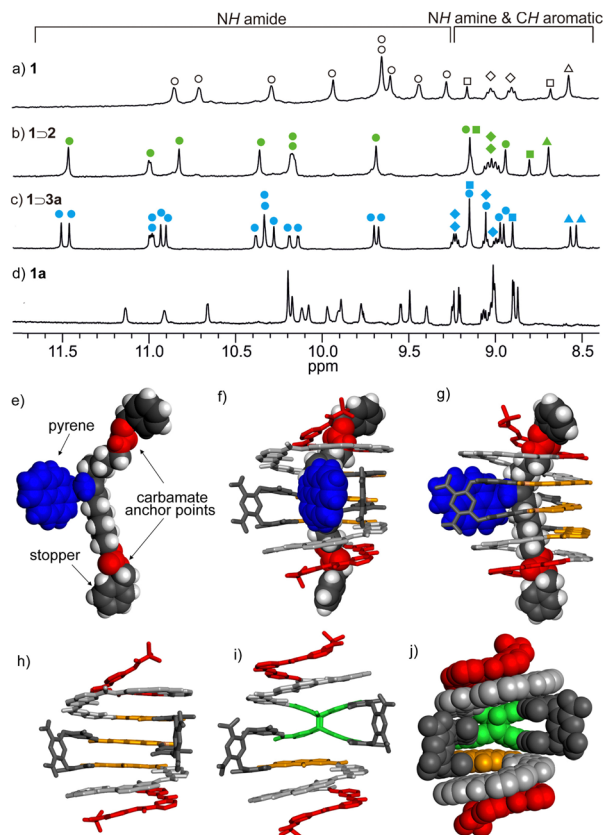


**Fig. 3** Part of the <sup>1</sup>H NMR spectra (CD<sub>2</sub>Cl<sub>2</sub>, 400 MHz) of: (a) 0.5 mM **1** in absence of guest; (b) 0.5 mM **1** in the presence of **2** (5 equiv.); (c) 0.5 mM **1** in the presence of **3a** (5 equiv.); (d) **1a**. NH amide protons, NH amine protons, CH aromatic protons from A<sup>H</sup> unit (H9 and H10) and H<sub>ext</sub> are marked as circles (O), diamonds (◊), squares (◻) and triangles (Δ), respectively. Signals of the free symmetrical host, symmetrical foldaxane **1**⊃**2** and unsymmetrical foldaxane **1**⊃**3a** are marked and filled with empty, green, and blue circles, respectively. Structures in the solid state analysed by X-ray crystallography of: (e) T-shape guest in the crystal packing; and (f) front view and (g) side view of foldaxane **1**⊃**3a**. The guest is shown as a CPK representation and the host is shown as a stick representation. (h) Host **1** as it exists in the structure of **1**⊃**3a**. Front view of the energy-minimised molecular models (using Merck molecular force field static, MMFFs) of **1a** in stick representation (i) and CPK representation (j). The carbamate and pyrene in the T-shape guest are marked in red and blue, respectively. The monomers in the host are colour coded as in Fig. 2. Side chains (O<sup>t</sup>Bu groups) of host and included solvent molecules have been removed for clarity.

In contrast, in the case of **3b** ( $\phi_F = 0.05$ ) at similar (sub-mM) concentration, non-structured emission was minimal (Fig. S6, ESI<sup>†</sup>), while at concentrations higher than 1 mM the excimer emission became increasingly intense.

Foldamer host **1** fluorescence was typically broad, short-lived and very weak ( $\phi_F = ca. 0.001$ , Fig. S7 and S8, ESI<sup>†</sup>), anthracene quenching being attributed to downhill electronic energy transfer. Diazaanthracene (A<sup>F</sup>-A<sup>H</sup>-A<sup>F</sup>) sub-units were integrated in the host capsule in a parallel orientation at distances (<4 Å) compatible with a A<sup>F</sup>-A<sup>H</sup> cycloisomerisation reaction, as shown in the single crystal X-ray structure (Fig. 3h). Diazaanthracene units have a high propensity to undergo homo- and hetero-photocyclisation reactions, often exhibiting

higher reaction quantum yields and resistance to secondary photoreactions than parent anthracene.<sup>3,15</sup> Photoirradiation of **1** in argon-bubbled halogenated solvents cleanly gave **1a** as denoted by shifting bridgehead proton resonances accompanying the C sp<sup>2</sup>-to-sp<sup>3</sup> conversion, notably the appearance of <sup>1</sup>H resonances between 5–5.5 ppm further exhibiting coupling with the fluorine, while the <sup>19</sup>F resonance at 160 ppm is characteristic of a photocyclised A<sup>F</sup>-A<sup>H</sup> pair of anthracenes (see Fig. S11 and S15, ESI<sup>†</sup>).<sup>3b</sup> The model of the photoproduct was obtained *via* molecular mechanics (Fig. 3i), revealing the formation of **1a** and 2 C–C bonds between the central anthracene A<sup>F</sup> and one of the A<sup>H</sup> central cycles. With photoproduct **1a** in hand, binding studies using either **1** or **1a** with threads were performed (Fig. S9, ESI<sup>†</sup>). While titrating guest **3a** with helix **1** in CH<sub>2</sub>Cl<sub>2</sub> led to a marked decrease of the exciplex emission ascribed to complexation (Fig. 4a;  $\phi_F$  dropping from 0.26 to 0.06), fluorescence emission showed virtually no capsule-induced quenching when adding **1a** (Fig. 4b), consistent with the absence of guest binding, further corroborated by NMR (Fig. S11–S13, ESI<sup>†</sup>). Consequently, photoswitching the foldaxane assembly would result in a lessened guest affinity and light-driven guest release. <sup>1</sup>H NMR spectroscopy showed that in **1**⊃**3a**, the cycloisomerised photoproduct was formed more slowly upon irradiation than in the free host **1** (Fig. 5a), as revealed by quantum yields obtained from photoconversion

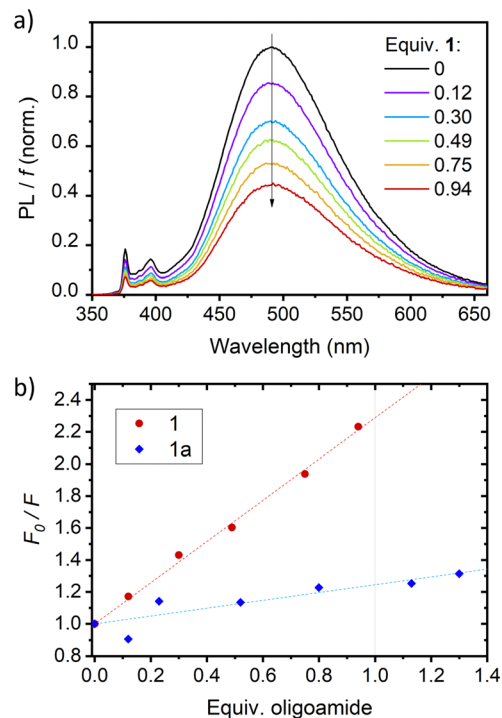


**Fig. 4** Quenching effect of host **1** on the fluorescence of a 0.5 mM solution of **3a** in CH<sub>2</sub>Cl<sub>2</sub> ( $\lambda_{exc} = 335$  nm) in the presence of Et<sub>3</sub>N (1.5 mM). (a) Fluorescence emission spectra of **3a** with increasing number of equivalents of **1** at constant volume, corrected by  $f$ , the amount of light absorbed by **3a** (see ESI<sup>†</sup>). (b) Quenching plots obtained upon addition of **1** or **1a** to **3a**.  $F$  is the integral of the corrected fluorescence, and  $F_0$  is the value measured in the absence of foldamer (lines are guides for the eye).



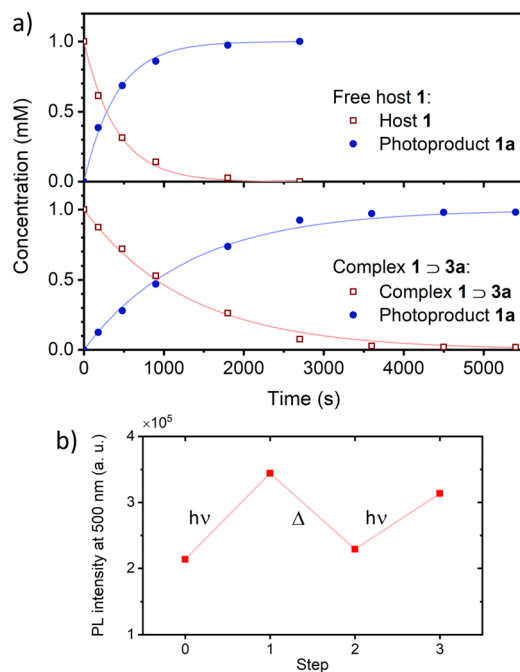


**Fig. 5** Release and uptake of guest **3a**. (a) Time evolution of the concentrations of the different species upon irradiation at 427 nm, as determined by  $^1\text{H}$  NMR ( $\text{CD}_2\text{Cl}_2 + 9 \text{ mM Et}_3\text{N}$ , 400 MHz). Top: Photoconversion of host **1** only; bottom: photoconversion of complex **1** to **3a**. In both cases, the experimental data were successfully fit to first order kinetics. (b) Release and uptake cycles performed in dichloroethane with fluorescence monitoring ( $\lambda = 500 \text{ nm}$ ).  $h\nu$ : irradiation at 427 nm;  $\Delta$ : heating at  $60^\circ\text{C}$  overnight.

kinetics fits ( $\phi_{\text{PC}} = 8.3 \times 10^{-4}$  and  $2.8 \times 10^{-4}$ , for **1** and **1** to **3a** respectively; Fig. S10, ESI $^\dagger$ ). The thermal reversibility of the reaction was further demonstrated, with the shifted proton resonances being restored to their original position on heating (Fig. S11 and S12, ESI $^\dagger$ ). Tests of reversible foldaxane assembly and disassembly cycles were carried out, and two full ejection-uptake cycles were successfully performed and monitored by NMR (Fig. S13, ESI $^\dagger$ ) and fluorescence switching (Fig. 5b), albeit with a small amount of unidentified secondary photoproduct.

In conclusion, a triple decker anthracene-containing foldamer capsule was designed and synthesised, which acted as a host for a T-shaped guest molecule. Photoirradiation of the host resulted in  $[4\pi+4\pi]$  photocyclisation within the capsule backbone, lowering guest affinity and provoking its photoejection. Thermal reversion of the supramolecular assembly in successive cycles was demonstrated, making this a unique example of a photo- and thermo-reversible foldaxane assembly. Further work is in progress to develop photoactivated foldaxane-based molecular machines.

Financial support from the China Scholarship Council, for a predoctoral fellowship (C. Y.), the French National Research Agency (grant ANR-18-CE6-0018, FORESEE) and the France-Germany International Research Project "Foldamers Structures and Functions" (IRP FoldSFun) are gratefully acknowledged. The work benefited from the facilities and expertise of the

Biophysical and Structural Chemistry platform at IECB, CNRS UMS3033, INSERM US001, Univ. Bordeaux.

The manuscript was written through contributions of all authors. All authors have given approval to the final version of the manuscript.

## Data availability

The data supporting this article have been included as part of the ESI $^\dagger$ . Crystallographic data for single crystals of **1** to **3a**, which were obtained *via* liquid-liquid diffusion, has been deposited at the CCDC under 2162063 (CIF in ESI $^\dagger$ ).

## Conflicts of interest

There are no conflicts to declare.

## Notes and references

- (a) D.-W. Zhang, X. Zhao, J.-L. Hou and Z.-T. Li, *Chem. Rev.*, 2012, **112**, 5271; (b) G. Guichard and I. Huc, *Chem. Commun.*, 2011, **47**, 5933; (c) T. A. Sobiech, Y. L. Zhong and B. Gong, *Org. Biomol. Chem.*, 2022, **20**, 6962; (d) K. M. Kim, G. Song, S. Lee, H.-G. Jeon, W. Chae and K.-S. Jeong, *Angew. Chem., Int. Ed.*, 2020, **132**, 22661.
- Y. Ferrand and I. Huc, *Acc. Chem. Res.*, 2018, **51**, 970.
- (a) B. Gole, B. Kauffmann, V. Maurizot, I. Huc and Y. Ferrand, *Angew. Chem., Int. Ed.*, 2019, **58**, 8063; (b) B. Gole, B. Kauffmann, A. Tron, V. Maurizot, N. McClenaghan, I. Huc and Y. Ferrand, *J. Am. Chem. Soc.*, 2022, **144**, 6894.
- V. Koehler, A. Roy, I. Huc and Y. Ferrand, *Acc. Chem. Res.*, 2022, **55**, 1074.
- (a) A. Petitjean, L. A. Cuccia, M. Schmutz and J.-M. Lehn, *J. Org. Chem.*, 2008, **73**, 2481; (b) T. A. Sobiech, Y. Zhong, L. S. Sanchez, B. B. Kauffmann, J. K. McGrath, C. Scalzo, D. P. Miller, I. Huc, E. Zurek, Y. Ferrand and B. Gong, *Chem. Commun.*, 2021, **57**, 11645; (c) Y. Zhong, T. A. Sobiech, B. Kauffmann, B. Song, X. Li, Y. Ferrand, I. Huc and B. Gong, *Chem. Sci.*, 2023, **14**, 4759.
- (a) R. S. Forgan, J. P. Sauvage and J. F. Stoddart, *Chem. Rev.*, 2011, **111**, 5434; (b) J. D. Crowley, S. M. Goldup, A. L. Lee, D. A. Leigh and R. T. McBurney, *Chem. Soc. Rev.*, 2009, **38**, 1530.
- (a) Q. Gan, Y. Ferrand, C. Bao, B. Kauffmann, A. Grélard, H. Jiang and I. Huc, *Science*, 2011, **331**, 1172; (b) X. Wang, B. Wicher, Y. Ferrand and I. Huc, *J. Am. Chem. Soc.*, 2017, **139**, 9350.
- (a) Q. Gan, X. Wang, B. Kauffmann, F. Rosu, Y. Ferrand and I. Huc, *Nat. Nanotechnol.*, 2017, **12**, 447; (b) S. A. Denisov, Q. Gan, X. Wang, L. Scarpantonio, Y. Ferrand, B. Kauffmann, G. Jonusauskas, I. Huc and N. D. McClenaghan, *Angew. Chem., Int. Ed.*, 2016, **55**, 1328.
- (a) L. Scarpantonio, A. Tron, C. Destribats, P. Godard and N. D. McClenaghan, *Chem. Commun.*, 2012, **48**, 3981; (b) P. R. Ashton, V. Balzani, O. Kocian, L. Prodi, N. Spencer and J. F. Stoddart, *J. Am. Chem. Soc.*, 1998, **120**, 11190.
- A. Lamouroux, L. Sebaoun, B. Wicher, B. Kauffmann, Y. Ferrand, V. Maurizot and I. Huc, *J. Am. Chem. Soc.*, 2017, **139**, 14668.
- C. Yao, B. Kauffmann, I. Huc and Y. Ferrand, *Chem. Commun.*, 2022, **58**, 5789.
- J. B. Birks, D. J. Dyson and I. H. Munro, *Proc. R. Soc. London, Ser. A*, 1963, **275**(1360), 575.
- (a) B. Daly, J. Ling and A. P. de Silva, *Chem. Soc. Rev.*, 2015, **44**, 4203; (b) A. P. de Silva, *J. Phys. Chem. Lett.*, 2011, **2**, 2865.
- (a) A. M. Swinnen, M. Van der Auweraer, F. C. De Schryver, K. Nakatani, T. Okada and N. Mataga, *J. Am. Chem. Soc.*, 1987, **109**, 321; (b) A. K. Purkayastha and S. Basu, *J. Photochem.*, 1979, **11**, 261.
- M. Li, A. D. Schlüter and J. Sakamoto, *J. Am. Chem. Soc.*, 2012, **134**, 11721.

